JVST A
Journal of Vacuum Science & Technology A

Thermally activated nucleation and growth of cobalt and nickel oxide nanoparticles on porous silica

Cite as: J. Vac. Sci. Technol. A **37**, 031101 (2019); https://doi.org/10.1116/1.5080448
Submitted: 08 November 2018 . Accepted: 04 March 2019 . Published Online: 03 April 2019

Vijayakumar Murugesan, Michel Gray, Mond Guo, Heather Job, Libor Kovarik, Arun Devaraj, Suntharampillai Thevuthasan, and Karthikeyan K. Ramasamy

Thermally activated nucleation and growth of cobalt and nickel oxide nanoparticles on porous silica

Vijayakumar Murugesan,[a] Michel Gray, Mond Guo, Heather Job, Libor Kovarik, Arun Devaraj, Suntharampillai Thevuthasan, and Karthikeyan K. Ramasamy[b]
Pacific Northwest National Laboratory, Richland, Washington 99354

(Received 8 November 2018; accepted 4 March 2019; published 3 April 2019)

Integrating mesoscale to the molecular level understanding of nanoparticle nucleation phenomena can drive the bottom-up synthesis approach for target applications. The authors studied the thermal evolution of binary metal oxide (cobalt and nickel oxides) nanoparticle structural phases on porous silica host from over wide spatial scale using multimodal analysis involving scanning transmission electron microscopy, x-ray absorption near-edge spectroscopy (XANES), and nuclear magnetic resonance (NMR) spectroscopy along with density functional theory (DFT) based calculations. The TEM analysis reveals thermally activated nanoparticle clustering and subsequent interaction with the porous host material. The Co and Ni K-edge XANES spectra revealed the evolution from metal hydroxide to metal oxide and subsequently metal silicate composites with calcination temperature. ^{29}Si NMR analysis revealed the role of surface functional groups of silica host for silicate composite formation, which is corroborated by DFT studies. *Published by the AVS.* https://doi.org/10.1116/1.5080448

I. INTRODUCTION

Atomic-level engineering of nanoparticles (NPs) with the ability to precisely tune its functional properties can help us realize many promising energy-related applications. Such a bottom-up approach would require a fundamental level understanding of nucleation and subsequent structural evolution of nanoparticles during the synthesis process. However, nanoparticle nucleation on a substrate from the solution phase relies on highly correlated processes involving reactive speciation pathways, molecular network formation, particle clustering, and preferential interaction with nucleation site. Metal oxide NPs are ubiquitous in modern devices, and the ability to control their functional properties through optimal structural designing can transform catalytic science. In particular, transition metal-based nanoparticles such as cobalt (Co), nickel (Ni), iron (Fe), palladium (Pd), and platinum (Pt) can serve as catalysts for many important reactions such as syngas conversion,[1,2] hydrogenation-dehydrogenation reactions,[3,4] and hydro-deoxygenation reactions.[5] The rate of catalytic reaction directly depends on a number of active sites, and this translates to achieving an optimal particle size (i.e., surface area) and a structural phase of the catalytic materials. Impregnating the catalytic material within porous support materials can inhibit agglomerated nanoparticle nucleation and thereby increase the surface area and subsequently catalytic active sites. However, dispersed metal/metal oxide catalytic systems over porous oxides (such as SiO_2, Al_2O_3, and TiO_2) exhibit complex nanostructures and its catalytic properties depend not only on particle size but also on the catalyst-support interfacial interactions. Porous SiO_2 is widely used as a support medium due to their chemical inertness under reducible and reactive chemical environments often encountered during the catalytic process.[6] Nevertheless, even chemically benign SiO_2 can have interaction with catalyst particles under high temperatures and adversely affect catalytic activity due to the presence of reactive surface functional groups.[7] Although the influence of the support on catalyst activity and the selectivity is widely studied with respect to the strong metal-support interaction and more recently on the electronic effect of metal-support interaction, the choice of support and the catalyst preparation method are still mostly determined by the empirical optimization.[8–10] Various structural and topological changes such as alloy formation, interdiffusion, and encapsulation can stem from the choice of the catalyst, support, and their treatment conditions.[7] Apart from the synthesis processes involving a cascade of chemical and thermal treatments, an exothermic catalytic process during system operation can also affect physiochemical properties of nanoparticles and their interactions with support materials. Hence, it is essential to understand the thermally induced nucleation of nanoparticles and their interaction with surface functional groups of support materials. For this study, we focus on the local structural evolution of cobalt and nickel oxide nanoparticles and their interaction with the SiO_2 support using the multimodal spectroscopic approach involving scanning transmission electron microscopy (STEM), x-ray absorption spectroscopy (XAS), nuclear magnetic resonance (NMR), and density functional theory (DFT) based computational methods.

II. EXPERIMENTAL DETAILS

The precursor materials are cobalt nitrate [$Co(NO_3)_2 \cdot 6H_2O$], nickel nitrate [$Ni(NO_3)_2 \cdot 6H_2O$], and Davisil Silica 645 (Sigma-Aldrich). The cobalt and nickel oxide nanoparticles are prepared as co-inhibit on the silica (SiO_2) support through the incipient wetness impregnation method. The appropriate quantities of both cobalt and a nickel nitrate solution were

Note: This paper is part of the Special Topic Collection on Complex Oxides.
[a]Electronic mail: Vijay@pnnl.gov
[b]Electronic mail: Karthi@pnnl.gov

combined with enough deionized water to bring the total volume of the impregnation solution to 90% of the water adsorption pore volume of the silica support (60/100 mesh, precalcined at 500 °C) to prepare the binary metal oxide nanoparticles. The solution was impregnated into the support in a drop-wise fashion on a vibrating table to keep the support solids in motion during impregnation. The impregnated catalysts were dried under an infrared lamp while being shaken until a steady weight was achieved, and then they were dried overnight at 110 °C in a drying oven. The dried catalysts were calcined at 350, 500, and 800 °C in air using a muffle furnace. To clearly rule out the effect of thermal annealing on silicon surface functional groups, we calcined the bare silica at 800 °C in an identical calcining condition and used as a pristine material for NMR and XAS analysis (*vide infra*).

X-ray powder diffraction (XRD) patterns of all calcined samples were recorded on a Phillips X-Pert (50 kV and 40 mA) diffractometer using Cu Kα radiation (λ¼ 1.54059 Å). Each sample was scanned in the range between 10° and 80°. STEM measurements were conducted with an FEI Titan 80-300 operated at 300 kV. The FEI Titan is equipped with a CEOS GmbH double-hexapole aberration corrector for the probeforming lens, which allows imaging with ~0.1 nm resolution in an STEM mode. The STEM images were acquired on a high angle annular dark field with an inner collection angle of 52 mrad. ^{29}Si NMR measurements were carried out using a Varian 300 MHz Infinity spectrometer ($B_0 = 7.05$ T and ^{29}Si Larmor frequency of 59.59 MHz). All the measurements were carried out under a magic angle spinning (MAS) speed of 5 kHz using tightly sealed 4 mm zirconia rotors. The ^{29}Si spectra were recorded using single pulse ^{29}Si MAS NMR experiments combined with high power ^{1}H decoupling at room temperature. Tetrakis(trimethylsilyl) silane {$[(CH_3)_3Si]_4Si$} was used as the secondary references for ^{29}Si (−9.8 ppm) relative to tetramethylsilane (0 ppm for ^{29}Si). The peak deconvolution and subsequent chemical shifts, linewidth, and integral intensity were obtained using the SPINWORKS program.[11]

Cobalt, nickel, and silicon K-edge x-ray absorption near-edge spectroscopy (XANES) measurements were performed at the Canadian Light Source beam-line port SXRMB. Co, Ni, and Si K-edge spectra were collected under a transmission mode, with powdered samples packed in multiple layers of a Kapton tape to ensure the sample uniformity. The oxygen and silicon K-edge spectra were collected using the scanning transmission x-ray microscopy (STXM) method at the Advanced Light Source, beam-line port 5.3.2.1. The O and Si K-edge spectra were measured by dispersing powder particles in silicon nitride windows, and the x-ray beam was focused on grain boundaries to probe the surface interactions. For all the XANES spectra, a linear background determined in the pre-edge region was subtracted from the raw data to correct the absorption from higher shells and from supporting materials.

Ground state DFT based calculations were carried out using the NWCHEM 6.6 package.[12] The hybrid-GGA based Becke, three-parameter, Lee-Yang-Parr (B3LYP) exchange-correlation functional with dispersion correction (DFT-D3) was employed for geometry and bonding energy calculations.[13–16] All the calculations reported herein were carried out using the ADZP basis set (double *Z*, double polarization function, all electron) with the Gaussian type functional taken from Environmental and Molecular Science Laboratory (EMSL) basis set exchange. Many recent studies focused on catalog of structures and energies of various $(SiO_2)_n$ clusters and reported that the most stable clusters found for $5 \leq n \leq 8$.[17,18] Hence, we choose an Si_8O_{12} nanocluster, which contains all the Q_2, Q_3, and Q_4 sites observed in our porous silica material.

III. RESULTS AND DISCUSSION

The nucleation of nanoparticles over a porous substrate is poorly understood, because of complexities associated with exogenous temperature, sporadic spatial confinement, and surface heterogeneities (such as surface defects and functional groups). The major challenge in gaining predictive understanding of the thermal evolution is to seamlessly access and integrating the necessary spatial regime, ranging from mesoscopic (~100 nm) to molecular level (~1 nm). Herein, we employed multimodal spectroscopy and microscopy along with the *ab-initio* level theory to gain an in-depth understanding of metal oxide evolution in the porous silica substrate.

A. Mesoscale structural and topographical evolution

Figure 1(a) shows XRD patterns of co-inhibiting cobalt and nickel oxide nanoparticles on silica substrates with 350, 500, and 800 °C heat treatments. Although XRD patterns are commonly used to fingerprint crystalline materials, phase identification of nanocrystalline metal oxide materials is complex due to inherent line broadening associated with structural distortion and smaller crystallites. In particular, differentiating the co-inhabitants (i.e., cobalt and nickel oxides) on the amorphous silicate support would be very complex as they adopt a similar structure and lattice constants [see Fig. 1(a)]. For example, both cobalt and nickel silicates exhibit a spinel structure with a very similar lattice constant (±0.1 Å) leading to XRD patterns with diminutive differences.[19] Similarly, the divalent cobalt and nickel oxides (CoO and NiO) exhibit a rock salt type cubit structure with similar lattice constants. It is proved to be challenging to clearly distinguish the crystalline phases of nanoparticles due to broader XRD patterns, which typically encompasses multiple structural patterns (see JCPDS data in Fig. 1). Nevertheless, it is evident that the widely reported binary metal oxides such as the $NiCo_2O_4$ spinel phase (JCPDS#200781) are not identified from the XRD pattern.[20] In particular, the absence of signature peaks of $NiCo_2O_4$ spinel phase high-temperature calcined samples clearly indicates that heterogeneous mixed oxide phases are minimal in the present materials. Beyond that, XRD patterns were not able to identify the disordered phases of metal oxides and hydroxide structures, which are ubiquitous in aqueous precipitation based synthesis methods. For example, in layered metal hydroxides such as α-$Co(OH)_2$, stacking faults and turbostratic disorder due to the presence of counter anions (Cl^-, NO_3^-, etc.) between the lamellae structure can cause broadened and asymmetric reflections leading to weak XRD patterns.[21–23]

The transmission electron microscope (TEM) analysis of various heat-treated cobalt and nickel oxide impregnated

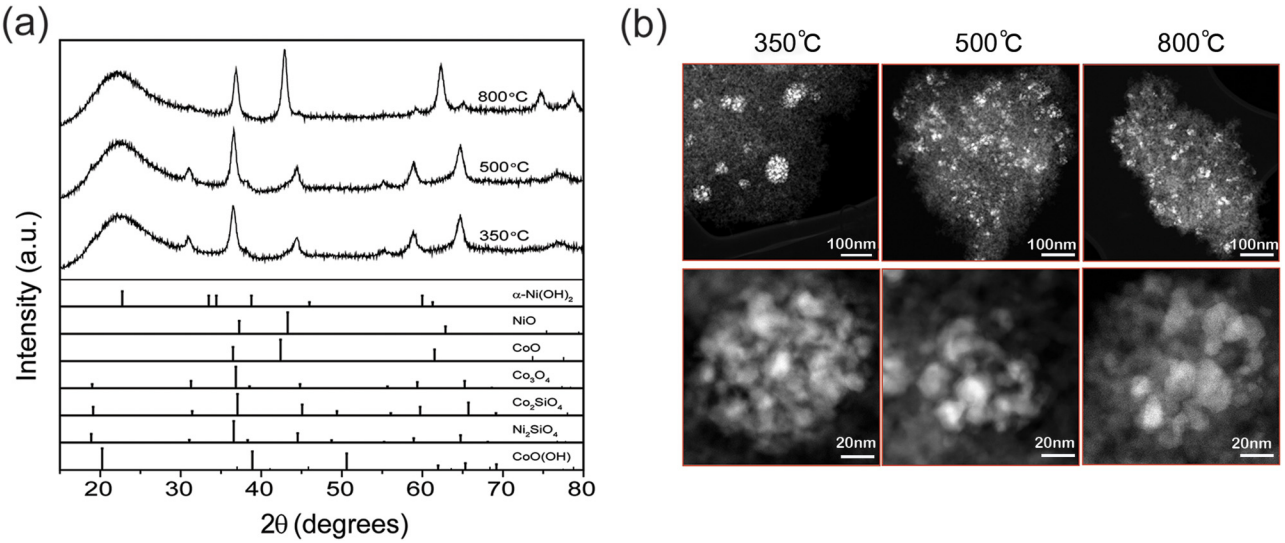

FIG. 1. (a) X-ray diffraction patterns of Co and Ni oxide impregnated silica particles calcined at 350, 500, and 800 °C along with relevant Co/Ni oxide and hydroxide patterns from JCPDS library. (b) Transmission electron microscope images of Co and Ni oxide impregnated silica particles calcined at different temperatures.

silica particles is shown in Fig. 1(b). Low-temperature (350 °C) thermal annealing leads to well-dispersed nucleation of nanoparticles (~10 nm), and with higher temperatures (500 and 800 °C), the clustering of nanoparticle effect is evident. The evolution of dispersed nanoparticles into clustering at elevated temperatures suggests a relatively weak interaction between silica host and impregnated metal oxide nanoparticles at low temperatures. This result is intriguing as the classical nucleation theory predicts that the nucleation barrier (ΔG) is smaller for heterogeneous nucleation along the surface of the host rather than homogeneous nucleation from the solution phase.[24] This implies the scarcity of preferential nucleation site within the host material, which can impose a homogeneous nucleation of metal oxides. With an increase in annealing temperature, the nucleated metal oxide particles can diffuse toward preferential sites within silica host and cluster together as part of heterogeneous nucleation. Such a thermally induced clustering and subsequent heterogeneous nucleation can cause host–guest interactions leading to unique crystalline phases. However, the traditional XRD analysis falls short of clearly identifying various crystalline phases due to intrinsic limitations as described earlier. Hence, it is necessary to use other molecular level spectroscopic probes, which can identify the atom specific local structure of metal oxide impregnated silica particles for better understanding about the thermal evolution process.

B. Fingerprinting the structural phase evolution

The chemical sensitivity of x-ray absorption near-edge structure (XANES) spectroscopy is well established and can be used to determine not only valence states but also coordination sites of metal species.[25,26] Figure 2(a) shows the Co K-edge XANES spectra of metal oxide impregnated silica particles with 350, 500, and 800 °C heat treatment along with respective metal oxides and precursor nitrate materials. The position of the main absorption peak (labeled as peak Co^{2+} and Co^{3+}) in the XANES spectra typically represents the oxidation state of the probing atom in the material. The precursor cobalt nitrate and cobalt oxide (CoO) representing the standard compounds for the Co^{2+} oxidation state registers the main absorption peak around 7725 eV, whereas the Co^{3+} oxidation state represented by cobalt oxide (Co_3O_4) registers a peak around 7730 eV. The metal oxide impregnated silica particles show multiple overlapping peaks in the main absorption range, indicating the presence of both Co^{2+} and Co^{3+} oxidation states in the heat-treated samples. Another important feature of the Co K-edge profiles is the small pre-edge peak (a few eV below the main K-edge absorption), which is suppressed with an increase in calcining temperatures. Typically, this pre-edge absorption peak represents a dipole-forbidden $1s \rightarrow 3d$ transition under specific coordination environments.[27]

For example, under tetrahedral coordination (T_d), the d_{xy}, d_{xz}, and d_{yz} orbitals will have t_2 symmetry similar to the *p*-orbitals due to lack of an inversion center, which can lead to a mixing of *d*-orbitals and *p*-orbitals and can register a strong pre-edge peak arising from the partially dipole allowed $1s \rightarrow 3d$ transition.[28] Similarly, structural distortion and vibrating local environments momentarily eliminating the centrosymmetry even under the symmetric octahedral environment (O_h) can also cause a weak pre-edge peak feature. Hence, the transition probability (peak intensity) of a pre-edge peak can be related to the coordination symmetry and also to the occupancy of the *3d* shell of a Co/Ni atom (i.e., oxidation state). The hexa-aqua cobalt nitrate [$Co(NO_3)_2 \cdot 6H_2O$] precursor material displays a weak pre-edge feature, indicating Co^{2+} in the slightly distorted octahedral environment (O_h). For low-temperature calcined (300 and 500 °C) samples, the pre-edge peak becomes more intense relative to the precursor nitrate, indicating noncentrosymmetric environment of tetrahedral cobalt (T_d).[29] As discussed earlier, the position of the main

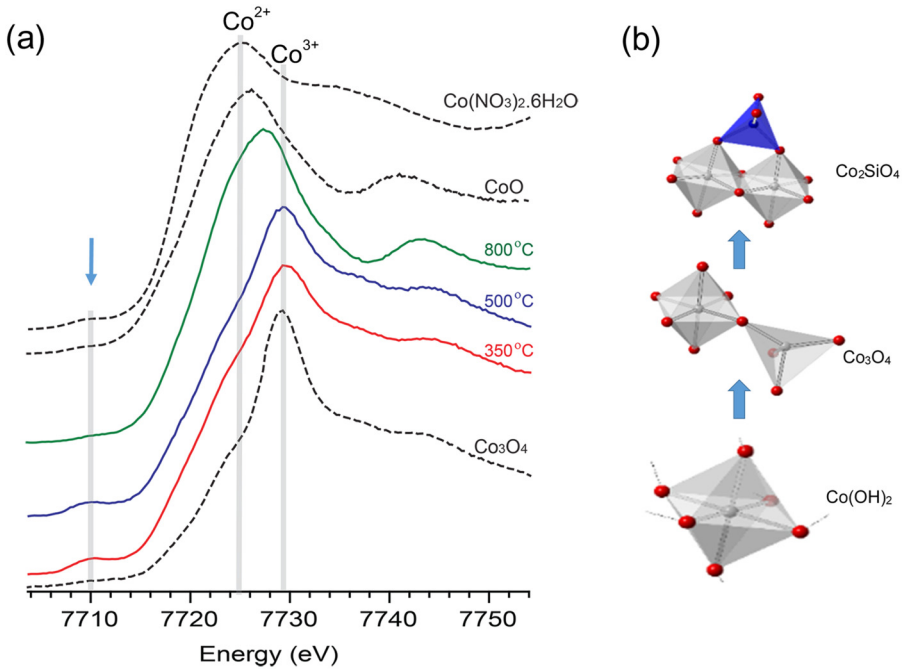

FIG. 2. (a) Co K-edge XANES spectra of metal oxide impregnated silica particles calcined at 350, 500, and 800 °C along with respective metal oxides and precursor nitrate materials (the arrow line indicates the pre-edge feature). (b) Schematic representation of cobalt local structure in the proposed solid phases of nanoparticles. Cobalt and silicon atoms are at the center of octahedral or tetrahedral structural units, which is defined by corner oxygen atoms. The hydrogen bonds are represented by dashed line.

absorption peak for low-temperature calcined samples indicates the presence of mixed cobalt oxidation with Co^{2+} and Co^{3+} as predominant and minor composition, respectively. Co_3O_4 is known as stable cobalt oxide which has the normal spinel structure, where two-thirds of Co^{3+} occupy octahedral positions and one-third of Co^{2+} occupies tetrahedral positions in the FCC oxygen lattice, and this tetrahedral Co^{2+} can cause the pre-edge peak. The calcined samples register similar XANES spectra as of the pure Co_3O_4, indicating the presence of Co_3O_4. Nevertheless, higher intensity of the pre-edge peak and the Co^{2+} main absorption peak relative to the Co_3O_4 model compound indicates a higher concentration of Co^{2+} species probably in a disordered tetrahedral environment in low-temperature calcined samples. The α-type cobalt hydroxide, i.e., $Co(OH)_2$, is known to show a strong pre-edge feature arising from distorted tetrahedral Co^{2+} at contribution along with the very weak (dipole forbidden) Co^{2+}octahedral contributions. Typically, the aqueous solvent based co-precipitation synthesis process for metal oxides involves a hydrolysis reaction with respective hydroxyl phases. For example, dissolution of cobalt/nickel nitrate precursor materials can produce hexa-aqua cobalt/nickel ions, which can donate hydrogen ions to water molecules in the solution due to their weak acidity,[30]

$$\left[M(H_2O)_6\right]^{2+}_{(aqu)} \rightarrow \left[M(H_2O)_4(OH)_2\right]^{0}_{(s)} + 2H^{+} \quad (M = Co/Ni). \tag{1}$$

This deprotonation induced hydroxide formation will be influenced by the counter anions along with the surface groups of host framework such as hydroxyl groups at silica surfaces (will be discussed later). The distorted hydroxide phase typically contains water molecules between octahedral oxygen sublattices, with little, or no, tendency to orient relative to one another leading to random layer orientation known as a "turbostratic structure."[21] In addition, frequent hydroxyl deficiency and/or trivalent cation substitution in the structure would lead to positively charged layers, in turn, leading to counter anion intercalation and subsequently an enhanced disordered type structure which may be silent in XRD analysis. For example, the α-type cobalt hydroxide may be formulated as $[Co^{2+}_{1-x}Co^{3+}_{x}(OH)_2]^{x+}[(NO_3)^{n-}_{x/n} \cdot mH_2O]$ with a mixed valence of Co^{2+} and Co^{3+} in tetrahedral and octahedral positions, respectively.[21,31,32] Hence, it is evident that the low-temperature calcining could cause the formation of disordered α-$Co(OH)_2$ along with Co_3O_4. It should be noted that the intensity of pre-edge peak drops with an increase in calcining temperature indicating a thermal evolution from α-type cobalt hydroxide to more stable Co_3O_4 phase, and in particular for high-temperature calcining (800 °C), the α-$Co(OH)_2$ composition is relatively minimal as evidenced by the drop in the pre-edge Co K-edge peak. Typically, the open-air calcining can cause cobalt hydroxide to oxidize into Co_3O_4 [as shown in Eq. (2)]. With an increase in calcining temperature, the oxidation reaction is more favored, causing the drop in $Co(OH)_2$ concentration at high-temperature calcined samples,

$$3Co(OH)_2 + \frac{1}{2}O_2 \rightarrow Co_3O_4 + 3H_2O. \tag{2}$$

Prolonged high-temperature calcining (800 °C) can cause the cobalt oxide to react with the silica network and form olivine

type Co_2SiO_4 composite materials.[33,34] In fact, the 800 °C calcined sample shows a significantly reduced pre-edge feature relative to low-temperature calcined samples [see Fig. 2(a)], and the overlapping main peaks indicate the presence of both Co^{2+} and Co^{3+} species. As discussed earlier, the pre-edge feature indicates the distorted tetrahedral Co(II) from the Co_3O_4 network, and hence the intensity loss clearly indicates the formation of a more ordered structure around Co^{2+} species. Esposito *et al.* reported that Co^{2+} species from the Co_3O_4 network can interact with surface hydroxyl groups of silica at higher temperatures and produce Co_2SiO_4 composite at interfaces.[34] It should be noted that Co_2SiO_4 contains only octahedral coordinated Co(II) within its crystal structure, indicating that tetrahedral Co(II) from the Co_3O_4 network turns into octahedral coordination by interacting with the silica surface [see Fig. 2(b)]. Loss of pre-edge peak intensity with an increase in calcining temperature shows a clear evidence of distorted tetrahedral Co^{2+} from Co_3O_4 network turning to a relatively ordered octahedral Co^{2+} structure as part of Co_2SiO_4 phase evolution. Hence, high-temperature calcining could result in a mixture of Co_3O_4 and Co_2SiO_4 phases. Such a thermally induced nucleation from a more disordered structural phase to a stable oxide phase follows Ostwald's step rule, which states that the crystallization from solution starts from the least stable to more stable polymorph structures.[35] However, it should be noted that the Co_2SiO_4 formation would depend not only on the calcining temperature but also on the relative concentration of Co_3O_4 phase and surface properties of the host silica network.[36] Possible interactions between cobalt species and host silica will be discussed later. Overall, the precursor hexa-aqua cobalt nitrate nucleates into disordered cobalt hydroxide and subsequent calcination leads to Co_3O_4 and Co_2SiO_4. We can now focus on the nickel oxide evolution using Ni K-edge XANES spectroscopy. Thermal evolution of nickel pre-edge feature resembles the cobalt K-edge spectra, indicating the presence of a disordered nickel site. Extending the previous argument of disordered metal hydroxide formation at low-temperature calcining, we can hypothesize the presence of disordered nickel hydroxide, i.e., $Ni(OH)_2$. Such a disordered nickel hydroxide phase might arise from (i) turbostratic structure where the interstratified motifs intercalated with water molecules and/or NO_3 anions, leading to $[Ni(OH)_{6-x}(NO_3)_x]$ or $[Ni(OH)_{6-x}(H_2O)_x]$ and (ii) the presence of nickel cation vacancies can cause compositional changes leading to a disordered phase such as $[Ni_{1-x}(OH)_{6-2x}(H_2O)_{2x}]$.[37–39] The other possibility of disordered structure might be the formation of nickel oxyhydroxide NiO(OH) with the Ni^{3+} oxidation state, which is also well reported in the literature. The Ni^{3+} ion in an NiO_6 octahedron will experience the Jahn–Teller effect owing to e_g^1 configuration, which can lead to octahedral distortion causing the pre-edge peak [see Fig. 3(b)]. On the other hand, Co^{3+} from analog cobalt oxyhydroxide CoO(OH) has e_g^0 configuration with no Jahn–Teller effect and subsequently no structural distortion in their octahedral sites. Although the pre-edge feature suggests that a distorted Ni octahedral site could also emerge from $Ni(OH)_2$ and/or NiO(OH) phases, lack of adequately resolved Ni(III) species in the main absorption peak suggests the disordered $Ni(OH)_2$ phase similar to the $Co(OH)_2$ phase discussed earlier. However, it should be noted that the literature reported that the main absorption energy difference between Ni(II) and Ni(III) is relatively small (~1.4 eV).[2,11,12]

Nevertheless, increasing calcination temperature reduces the pre-edge peak intensity as well as the linewidth of the main absorption peak indicating Ni(II) species in the well-ordered octahedral environment as expected of the NiO material. In

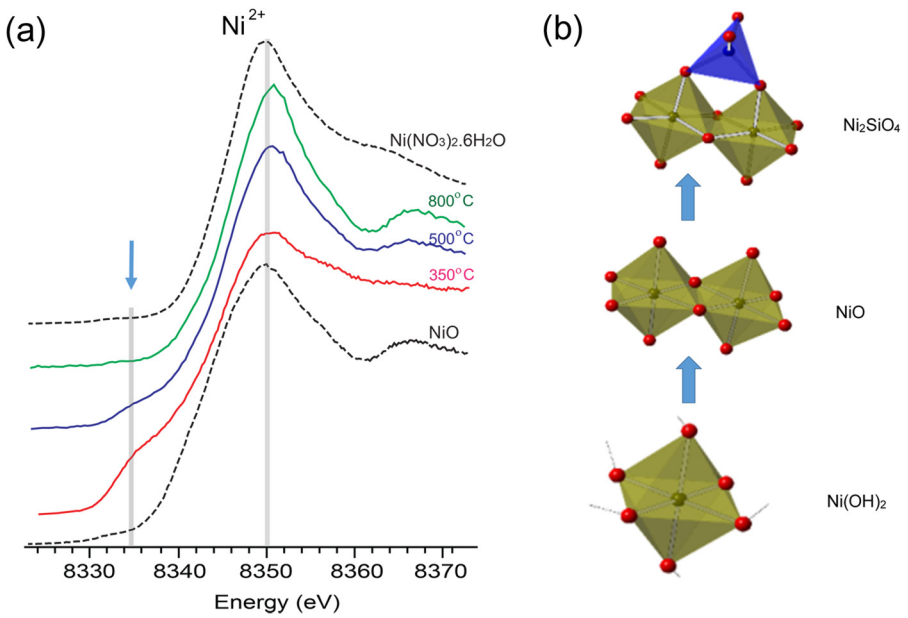

FIG. 3. (a) Ni K-edge XANES spectra of metal oxide impregnated silica particles calcined at 350, 500, and 800 °C along with respective metal oxides and precursor nitrate materials (the arrow line indicates the pre-edge feature). (b) Schematic representation of cobalt local structure in the proposed solid phases of nanoparticles. Nickel and silicon atoms are at the center of octahedral and tetrahedral structural units respectively. The oxygen atoms are at the corner of these structural units. The hydrogen bonds are represented by dashed line.

fact, it is known that $Ni(OH)_2$ decomposes into stable NiO at 400 °C as shown in the following equation:[40]

$$Ni(OH)_2 \rightarrow NiO + H_2O. \quad (3)$$

Like cobalt oxide, nickel oxide can also form Ni_2SiO_4 composite materials by interacting with silica host at high-temperature calcining. Nevertheless, it would be challenging to clearly distinguish Ni_2SiO_4 and NiO phases as both structures have Ni(II) in the octahedral symmetry. Overall, both cobalt and nickel species nucleate into disordered hydroxide phase and subsequently oxidized and hydrolyzed to Co_3O_4 and NiO, respectively. With high-temperature calcining, these metal oxides can react with silica host and form metal silicate-type composite material, which depends on the surface properties of silica host, in particular, hydroxyl functional groups.

C. Metal oxide interaction with silica host

With the acquired knowledge about structural phase evolution within metal oxide nanoparticles, we can now focus on their interaction with the host (i.e., porous silica) during the calcining process. We measured oxygen K-edge spectroscopy of metal oxide impregnated silica particles prepared under various calcination temperatures. The STXM enables the region-specific XANES analysis by using a focused x-ray beam at the grain boundaries and helps us inhibit the signals from an ubiquitous oxygen-containing support material common in traditional XAS measurements. Nevertheless, our attempts to analyze the metal oxide–silica interfacial interaction were proved to be challenging due to a very low concentration (~6%) and a smaller particle size (<20 nm) of metal oxide particles leading to overwhelming signal from bare silica. The oxygen K-edge XANES spectra collected from the STXM measurements are shown in Fig. 4. A very low-intensity peak around 532 eV representing cobalt and nickel oxides is observed. Such a low-intensity peak proved to be challenging in analyzing the structural phase evaluation of metal oxides. In addition, the major peak around 538 eV representing silica is broad and poor resolution further restrain gaining qualitative analysis of silica surface–metal oxide interactions. Overall, even under STXM mode, both oxygen and silicon K-edge spectra lack the necessary spatial resolution for analyzing low concentration metal oxide nanoparticles in the silica support.

On the other hand, such a low metal oxide impregnation on silicon pores might be probed by solid-state NMR examination of host and guest interfacial interactions. In particular, the higher surface area of porous silica can provide a sufficient number of silicon nuclei and hydroxyl functional groups to achieve cross polarization (CP) based solid-state NMR measurements. Figure 5 shows ^{29}Si CP-MAS NMR spectra of calcined (800 °C) silica and metal oxide impregnated silica particles calcined at 350, 500, and 800 °C. The calcined silica host material shows a high intensity peak around −100 ppm, representing Q_3 single silanols unit of surface $(Si–O–)_3$**Si**–OH groups and two low-intensity peaks around −110 and −90 ppm peak, representing Q_4 siloxane

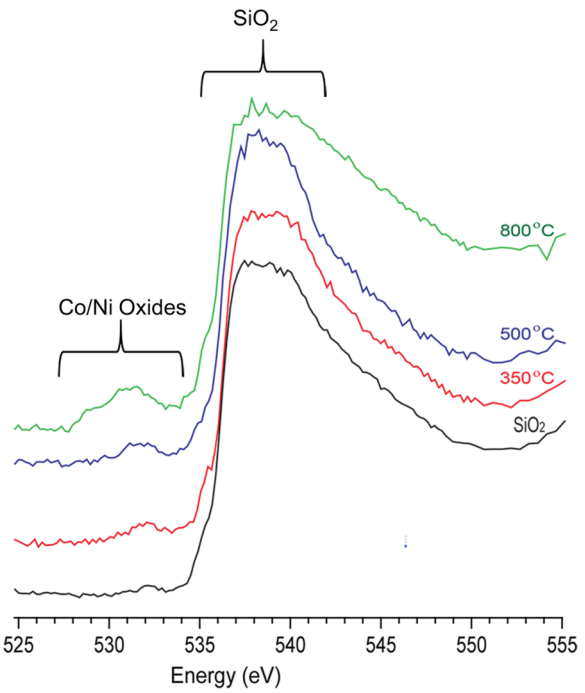

FIG. 4. Oxygen K-edge XANES spectra collected under STXM mode of metal oxide impregnated silica particles calcined at 350, 500, and 800 °C along with pristine porous silica materials [see supplemental material (Ref. 43) for further details].

unit of surface $(Si–O–)_4$**Si** groups and Q_2 geminal silanols unit of surface $(Si–O–)_2$**Si**–$(OH)_2$ groups, respectively [see Fig. 4(b)].[41,42] Porous silica impregnated with Co and Ni oxide under the low-temperature (350 and 500 °C) calcining process resembles the pristine silica albeit small line broadening in Q_4 siloxane and Q_2 geminal silanol groups. It is known that the increase in ^{29}Si NMR linewidth typically represents structural disorder in terms of Si–O bond lengths and angles.[42] For example, thermal calcination under open-air conditions can cause the dangling hydroxyl bonds from silanol groups on silica surfaces to interact with nitrate counter anions and residual water molecules. Such interactions can cause multiple conformations with nonuniform Si–OH bond angles and/or bond distances which can manifest as ^{29}Si NMR line broadening owing to the distribution of isotropic chemical shifts. In addition, dangling hydroxyl bonds from silanol groups can also act as an active and/or nucleation site for the growth of cobalt and nickel oxide particles. For the latter instance, the paramagnetic interactions arising from unpaired electrons of cobalt and nickel atoms of respective oxides/hydroxides can cause a hyperfine chemical shift in addition to linewidth broadening from conformation based chemical shift distributions. The magnitude of hyperfine chemical shift will critically depend on the bonding distance between observing silicon atom and cobalt/nickel atomic sites and hence serve as an effective local probe to identify the nucleation site within silica surface groups. Overall, the interaction of paramagnetic metal centers with silica surface will induce significant changes to ^{29}Si NMR peaks. However, for low-temperature calcination (350 and 500 °C) all the ^{29}Si NMR peaks register relatively smaller

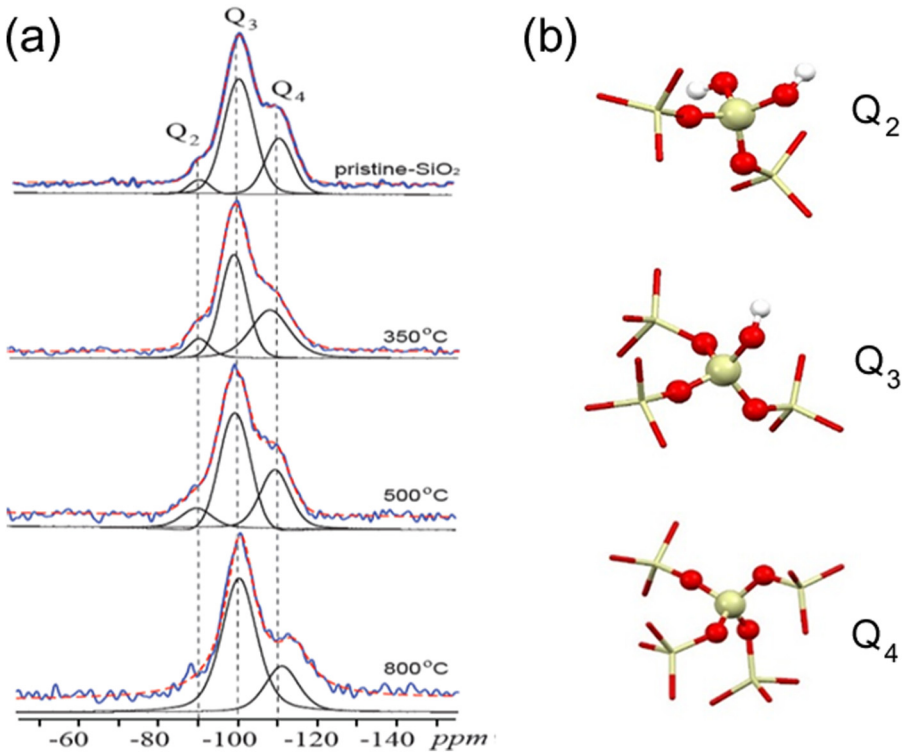

FIG. 5. (a) Proton cross-polarized (CP) ^{29}Si MAS NMR spectra of calcined (800 °C) silica and metal oxide impregnated silica particles calcined at 350, 500, and 800 °C. (b) Schematic representation of Q_2, Q_3 silanol, and Q_4 siloxane groups of silica host. The primary SiO_4 groups (Q_2,Q_3 and Q_4) and dangling hydrogen are represented in balls and stick representation, whereas the extended silica structures were shown in stick representation.

line broadening and chemical shift changes indicating the weaker interaction between the metal oxide nucleates and the silica surface. This is intriguing, considering the acidic nature of the hexa-aqua cobalt/nickel complex, it is expected to undergo a hydrolysis reaction with hydroxyls of silanol groups (Q_2 and Q_3) and initiate the nucleation process as shown in the following equations:

$$(O_3{-}Si){-}OH + [M \cdot 5H_2O \cdot OH]^+ \rightarrow O_3{-}Si - O - M \cdot 5H_2O + H_2O(M = \text{Co or Ni}), \quad (4)$$

$$(Si - O{-})_2Si{-}(OH)_2 + [M \cdot 5H_2O \cdot OH]^+ \rightarrow (Si - O{-})_2{-}OH - Si{-}O_1{-} M \cdot 5H_2O + H_2O\,(M = \text{Co or Ni}). \quad (5)$$

However, it should be noted that surface hydroxyl groups are also prone to interact with nitrate counter ions than the acidic aqua-metal cations. Such an interaction could explain the observed NMR line broadening in low-temperature calcined samples. Further heat treatment caused the Q_2 peak intensity greatly suppressed, indicating significant line broadening effect possibly arising from the paramagnetic metal center interaction. This is in agreement with XANES analysis discussed earlier, where the high-temperature calcination leads to the composite formation (such as Co_2SiO_4 and Ni_2SiO_4). Under these composite formations, the silicon tetrahedral units will have corner sharing structural arrangement with Co/Ni octahedral units. This could cause a significant paramagnetic induced chemical shift and linewidth changes as observed in Q_2 silanol groups under the high-temperature calcined sample. Nevertheless, it is intriguing that the Q_3 and Q_4 groups register only a marginal linewidth change similar to low-temperature calcined samples. This indicates that the Q_2 silanol groups are directly participating in the metal silicate formation at host-metal oxide interfaces, despite their relatively lower concentration than Q_3 silanol groups [see Fig. 5(a)].

To further analyze the porous silica host and aqueous metal ion interactions, we performed DFT based quantum calculations. The silica nanoclusters (Si_8O_{12}) with silanol Q_2 and Q_3 hydroxyl groups are used as a model for the silica host material. Since the Q_4 siloxane group does not have any hydroxyl group and present only in the near-surface and bulk region, we focus on more surface active silanol Q_2 and Q_3 groups. This assumption is also supported by our ^{29}Si CP-MAS NMR experiments discussed earlier. The hexa-aqua cobalt/nickel ions, i.e., $(Co/Ni{\cdot}6H_2O)^{2+}$ were used as a metal oxide model to understand the host–nanoparticle interactions. The hexa-aqua ions were placed near Q_2 and Q_3 groups and optimized without any further constraints. Figure 6 shows the optimized structure of hexa-aqua cobalt ions interactions with Q_2 and Q_3 silanol groups of silica clusters. Molecular structural optimization was performed by placing the hexa-aqua metal ion species bonded with hydroxyl groups of silanol group.

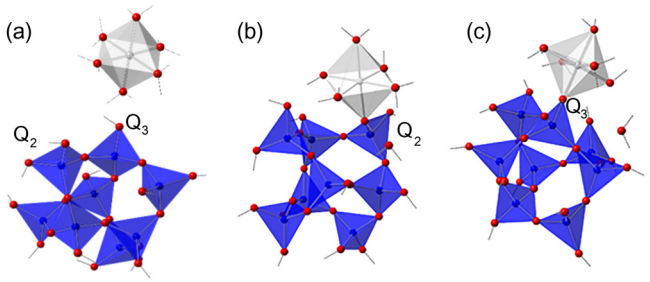

FIG. 6. Density functional theory optimized structure of (a) silica nanocluster (Si_8O_{12}) and hexa-aqua cobalt ion ($[Co \cdot 6H_2O]^{2+}$), (b) hexa-aqua cobalt ion ($[Co \cdot 6H_2O]^{2+}$) interaction with Q_2 silanol group, (c) hexa-aqua cobalt ion ($[Co \cdot 6H_2O]^{2+}$) interaction with Q_3 silanol group. Cobalt, oxygen, and silicon atoms are represented as gray, red, and blue spheres, respectively, whereas the hydrogen bonds are represented as a dashed line.

During optimization, an axial water molecule moved away from metal ion species and established hydrogen bonding with other hydroxyl groups of silica indicating the possibility of silicate composite formation discussed from experimental results. To explore the possibility of preferential nucleation site within silica host, we calculated the respective bonding energies for Q_2 and Q_3 silanol groups. The bonding energy requirements were calculated as the difference between bonding energy of the individual products (i.e., silica cluster and hexa-aqua ions) and resultant molecules (see Fig. 6). The calculated bonding energy requirements reveal that both cobalt (II) and nickel (II) aqua ions show similar bonding energies (±0.1 eV) for their interaction with silica host. In addition, both cobalt and nickel aqua ions register favorable bonding energy (~0.20 eV) with the Q_2 silanol group than the Q_3 silanol group. This result is in agreement with our ^{29}Si CP-MAS NMR experiments discussed earlier. However, it should be noted that the smaller bonding energy difference between Q_2 and Q_3 silanol groups means Q_3 can also act as a nucleation site for metal oxide nanoparticles albeit little less favorably than the Q_2 sites. This could explain the heterogeneous nucleation initiated at elevated thermal treatment discussed earlier in TEM analysis. Overall, the combined multimodal analysis reveals that nucleation of metal oxide nanoparticles within the porous host is a complicated process, which heavily relies on the preferential nucleation site and crystalline phase evolution probabilities of the metal oxides.

IV. SUMMARY AND CONCLUSIONS

The structural evolution of co-inhibiting cobalt and nickel oxide nanoparticles in the porous silica support during thermal treatment was investigated with mesoscale (XRD and STEM) and molecular (XANES and NMR) spectroscopy along with DFT calculations. The mesoscale analysis reveals thermally induced clustering phenomena and subsequent host–guest interactions. Nevertheless, it lacks quantitative assessment about the chemical interactions. The molecular level view is accessed through Co and Ni K-edge XANES analysis, which revealed that low-temperature calcining causes disordered Co/Ni hydroxide phase which evolves from nitrate precursors and is subsequently oxidized to respective metal oxides due to open-air heat treatment. The further treatment causes metal silicate composite formation due to silica–metal oxide interfacial interactions. ^{29}Si NMR analysis revealed that Q_2 silanol groups are the relatively preferential site for silicate composite formation. The DFT studies also predicted that the Q_2 silanol groups are slightly more energetically favorable than other silanol groups for the silicate composite. Thus, we have shown that metal oxide nanoparticle evolution is depending on both thermal treatment and host–metal oxide interfacial interactions using multimodal analysis which probes a wide spatial regime from mesoscale to molecular scale. Undoubtedly, further studies are necessary for quantitative descriptions and predictive understanding about the role of the preferential host site and guest molecule interactions.

ACKNOWLEDGMENTS

The synthesis, NMR, and computational work were financially supported by the U.S. Department of Energy (DOE) Bioenergy Technology Office (BETO) and performed at Pacific Northwest National Laboratory (PNNL). PNNL is operated by the Battelle Memorial Institute for the U.S. DOE under Contract No. DE-AC05-76RL01830. The XAS measurements were supported by PNNL-chemical imaging initiative LDRD program. The STEM, NMR, and DFT computation work were carried out at EMSL (www.emsl.pnl.gov), a national scientific user facility sponsored by the DOE's Office of Biological and Environmental Research. The XAS analysis was performed at Canadian Light Source (CLS), a national scientific user facility which is supported by the Natural Sciences and Engineering Research Council of Canada. The STXM measurements were performed at Advanced Light Source, which is a DOE Office of Science User Facility under Contract No. DE-AC02-05CH11231.

[1]K. Takanabe, K. Nagaoka, K. Nariai, and K. Aika, J. Catal. **232**, 268 (2005).
[2]K. K. Ramasamy, M. Gray, H. Job, and Y. Wang, Chem. Eng. Sci. **135**, 266 (2015).
[3]T. Fujikawa, K. Idei, T. Ebihara, H. Mizuguchi, and K. Usui, Appl. Catal. A Gen. **192**, 253 (2000).
[4]M. M. Bhasin, J. H. McCain, B. V. Vora, T. Imai, and P. R. Pujado, Appl. Catal. A Gen. **221**, 397 (2001).
[5]E. Furimsky, Appl. Catal. A Gen. **199**, 147 (2000).
[6]R. Lamber and W. Romanowski, J. Catal. **105**, 213 (1987).
[7]B. K. Min, A. K. Santra, and D. W. Goodman, Catal. Today **85**, 113 (2003).
[8]G. R. Jenness and J. R. Schmidt, ACS Catal. **3**, 2881 (2013).
[9]S. J. Tauster, Acc. Chem. Res. **20**, 389 (1987).
[10]C. T. Campbell, Nat. Chem. **4**, 597 (2012).
[11]K. Marat, SPINWORKS (University of Manitoba, Manitoba, 2009), see https://home.cc.umanitoba.ca/~wolowiec/spinworks/index.html.
[12]G. te Velde, F. M. Bickelhaupt, E. J. Baerends, C. Fonseca Guerra, S. J. A. van Gisbergen, J. G. Snijders, and T. Ziegler, J. Comput. Chem. **22**, 931 (2001).
[13]S. Grimme, J. Antony, S. Ehrlich, and H. Krieg, J. Chem. Phys. **132**, 154104 (2010).
[14]A. D. Becke, Phys. Rev. A **38**, 3098 (1988).
[15]C. Lee, W. Yang, and R. G. Parr, Phys. Rev. B **37**, 785 (1988).
[16]S. Grimme, W. Hujo and B. Kirchner, Phys. Chem. Chem. Phys. **14**, 4875 (2012).
[17]S.-X. Hu, J.-G. Yu, and E. Y. Zeng, J. Phys. Chem. A **114**, 10769 (2010).
[18]J. A. W. Harkless, D. K. Stillinger, and F. H. Stillinger, J. Phys. Chem. **100**, 1098 (1996).

[19]T. Yagi, F. Marumo, and S. I. Akimoto, Am. Mineral. **59**, 486 (1974), available at https://pubs.geoscienceworld.org/msa/ammin/article-abstract/59/5-6/486/541074/crystal-structures-of-spinel-polymorphs-of-fe2sio4?redirectedFrom=fulltext.
[20]D. P. Dubal, P. Gomez-Romero, B. R. Sankapal, and R. Holze, Nano Energy **11**, 377 (2015).
[21]D. S. Hall, D. J. Lockwood, C. Bock, and B. R. MacDougall, Proc. R. Soc. A Math. Phys. Eng. Sci. **471**, 20140792 (2015).
[22]M. B. Davies and J. W. Lethbridge, J. Inorg. Nucl. Chem. **34**, 2171 (1972).
[23]L. Markov, K. Petrov, and V. Petkov, Thermochim. Acta **106**, 283 (1986).
[24]S. Karthika, T. K. Radhakrishnan, and P. Kalaichelvi, Cryst. Growth Des. **16**, 6663 (2016).
[25]A. Bordage, V. Trannoy, O. Proux, H. Vitoux, R. Moulin, and A. Bleuzen, Phys. Chem. Chem. Phys. **17**, 17260 (2015).
[26]C. Garino, E. Borfecchia, R. Gobetto, J. A. van Bokhoven, and C. Lamberti, Coord. Chem. Rev. **277–278**, 130 (2014).
[27]F. de Groot, G. Vankó, and P. Glatzel, J. Phys. Condens. Matter **21**, 104207 (2009).
[28]T. E. Westre, P. Kennepohl, J. G. DeWitt, B. Hedman, K. O. Hodgson, and E. I. Solomon, J. Am. Chem. Soc. **119**, 6297 (1997).
[29]T. Yamamoto, X-Ray Spectrom. **37**, 572 (2008).
[30]M. D. Alba, A. I. Becerro, M. A. Castro, A. C. Perdigón, and J. M. Trillo, J. Phys. Chem. B **107**, 3996 (2003).
[31]J. R. Neilson, B. Schwenzer, R. Seshadri, and D. E. Morse, Inorg. Chem. **48**, 11017 (2009).
[32]R. Ma, Z. Liu, K. Takada, K. Fukuda, Y. Ebina, Y. Bando, and T. Sasaki, Inorg. Chem. **45**, 3964 (2006).
[33]M. Stoia, M. Stefanescu, T. Dippong, O. Stefanescu, and P. Barvinschi, J. Sol-Gel Sci. Technol. **54**, 49 (2010).
[34]S. Esposito, M. Turco, G. Ramis, G. Bagnasco, P. Pernice, C. Pagliuca, M. Bevilacqua, and A. Aronne, J. Solid-State Chem. **180**, 3341 (2007).
[35]W. Ostwald, Z. Phys. Chem. **22**, 289 (1897).
[36]N. T. K. Thanh, N. Maclean, and S. Mahiddine, Chem. Rev. **114**, 7610 (2014).
[37]T. N. Ramesh, J. Phys. Chem. B **113**, 13014 (2009).
[38]A. Van der Ven, D. Morgan, Y. S. Meng, and G. Ceder, J. Electrochem. Soc. **153**, A210 (2006).
[39]A. J. Tkalych, K. Yu, and E. A. Carter, J. Phys. Chem. C **119**, 24315 (2015).
[40]Z.-H. Liang, Y.-J. Zhu, and X.-L. Hu, J. Phys. Chem. B **108**, 3488 (2004).
[41]T. Tsuboi, T. Sakka, and Y. H. Ogata, Phys. Rev. B **58**, 13863 (1998).
[42]R. Faulkner, J. DiVerdi, Y. Yang, T. Kobayashi, and G. Maciel, Materials **6**, 18 (2013).
[43]See supplementary material at https://doi.org/10.1116/1.5080448 for Silicon and Oxygen K-edge XANES spectra collected under scanning transmission X-ray microscopy (STXM) mode.